# Characterization and Implementation of Dual-SiC MOSFET Modules for Future Use in Traction Converters

Joseph Fabre, Philippe Ladoux, *Member, IEEE*, and Michel Piton

***Abstract*—Silicon (Si) insulated-gate bipolar transistors are widely used in railway traction converters. In the near future, silicon carbide (SiC) technology will push the limits of switching devices in three directions: higher blocking voltage, higher operating temperature, and higher switching speeds. The first silicon carbide (SiC) MOSFET modules are available on the market and look promising. Although they are still limited in breakdown voltage, these wide-bandgap components should improve traction-chain efficiency. Particularly, a significant reduction in the switching losses is expected which should lead to improvements in power–weight ratios. Nevertheless, because of the high switching speed and the high current levels required by traction applications, the implementation of these new modules is critical. An original method is proposed to compare, in terms of stray inductance, several dc bus-bar designs. To evaluate the potential of these new devices, a first set of measurements, based on a single-pulse test-bench, was obtained. The switching behavior of SiC devices was well understood at turn-off and turn-on. To complete this work, the authors use an opposition method to compare Si-IGBT and SiC-MOSFET modules in voltage source inverter operation. For this purpose, a second test-bench, allowing electrical and thermal measurements, was developed. Experimental results confirm the theoretical loss-calculation of the single-pulse tests and the correct operation of up to three modules directly connected in parallel. This analysis provides guidelines for a full SiC inverter design, and prospects for developments in traction applications are presented.**

***Index Terms*—Loss measurement, power MOSFET, power semiconductor devices, silicon carbide, switching loss.**

## I. Introduction

NOW, power electronics has used silicon components. Developed almost 30 years ago [1], [2], IGBTs arrived in railway traction converters in 1992 [3] and quickly supplanted earlier bipolar devices such as phase-controlled thyristors or GTOs. While improvements continue to be made [4–10], silicon technology is reaching an asymptote and progress on breakdown-voltage and switching performance is limited (see Fig. 1).

Recently, some semiconductor manufacturers began the production of SiC transistors with a breakdown voltage of 1200 V or even 1700 V. These components are marketed in single-chip devices and/or in power modules [11], [12]. For ten years, many publications showed that SiC devices are very attractive in terms of blocking voltage [13–15], operating temperature [16–18], and switching frequency [19–21] which is why traction-drive manufacturers now have to seriously consider this new technology [22–27]. At the moment, some suppliers are offering silicon carbide (SiC) MOSFET modules [28–32] which seem very promising to improve traction drive performance. The first commercial 1200 V-100 A dual-SiC MOSFET modules essentially push the limits of switching speeds and allow an increase of converter efficiency. To evaluate the potential of these new devices, a first set of measurements, based on a single and double-pulse test-bench (chopper with inductive load), was achieved [33]. However, these tests require sensors with large bandwidths [33], and it is difficult to obtain accurate measurements of switching energies from current and voltage waveforms. Nevertheless, they help to understand turn-off and turn-on behavior and the impact of the electrical environment (parasitic *RLC*) on the switching waveforms. To go further in the characterization of these modules, the authors proposed a second step using the opposition method [34], [35] to compare Si-IGBT and SiC-MOSFET modules in voltage source inverter (VSI) operation [36]. Different methods for estimating semiconductor losses have been implemented on the test-bench, and experimental results with Si-IGBTs and SiC-MOSFETs have been presented and compared [36]. They clearly show the attractiveness of SiC-MOSFETs with regards to increased efficiency and/or weight and volume reduction of traction chains.

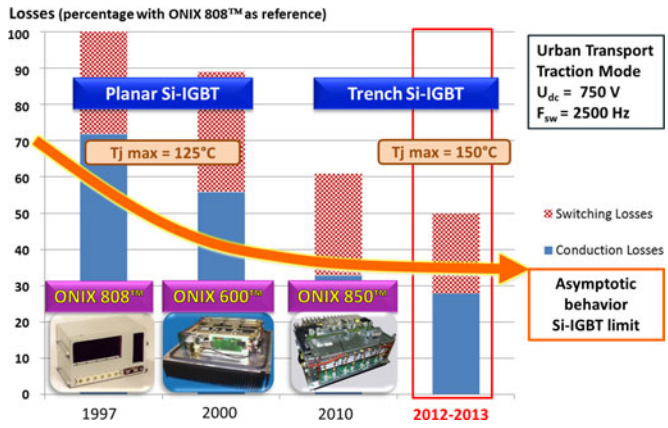


Fig. 1. ALSTOM Transport, urban traction converter losses versus time and Si-IGBT technologies.

Manuscript received April 24, 2014; revised July 21, 2014; accepted August 20, 2014. Date of publication August 27, 2014; date of current version March 5, 2015. Recommended for publication by Associate Editor A. Lindemann.

J. Fabre and P. Ladoux are with ENSEEIHT, LAPLACE, Toulouse 31071, France (e-mail: joseph.fabre@laplace.univ-tlse.fr; philippe.ladoux@laplace.univ-tlse.fr).

M. Piton is with the Department of Engineering, ALSTOM Transport, Semeac 65601, France (e-mail: michel.piton@transport.alstom.com).

Color versions of one or more of the figures in this paper are available online at http://ieeexplore.ieee.org.

Digital Object Identifier 10.1109/TPEL.2014.2352863

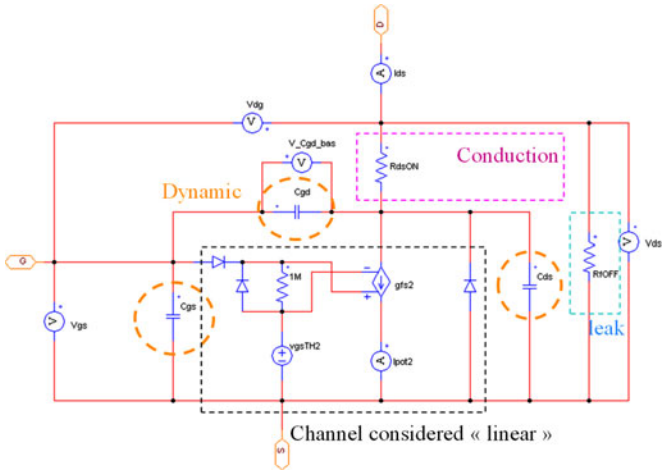


Fig. 2. SiC-MOSFET macro model developed in PSIM software.

Study and implementation of dual-SiC MOSFET modules for traction converters is not straightforward, and the aim of this paper is to show how this can be done.

## II. Key to Understanding SiC Switching in Its Environment and Its Implementation: Device Modeling

### A. Macrobehavioral Models and Switching Simulations of 1200 V-100 A Dual-SiC MOSFET Modules

Simulations are needed to completely understand the switching waveforms. To this effect, the behavioral model of a SiC-MOSFET was developed in PSIM software. This macro model allows a first approximation and analysis of the different stages during turn-on and turn-off. It will also be used for modeling components in their environment (see Section II-B.). This macro model for a SiC-MOSFET was built with the use of a classical Si Power MOSFET modeling tool. It is easier and faster to implement than the physical model based on analytical diffusion equations and for which the manufacturer's proprietary data is unavailable. The behavioral model parameters are easily extracted from manufacturer's data ($R_{\mathrm{dsON}}, V_{\mathrm{gsTH}}, g_{\mathrm{fs}}, \ldots$) and can be refined by component measurements. This model, shown in Fig. 2, has a linear channel opening and constant parasitic capacitances. Polynomial modeling of an open channel, not detailed here, was implemented.

The simulations have to be performed in the same conditions as the practical tests which follow (see Fig. 10). To this effect, the modeling, which includes a macro model of the antiparallel diode, considers a chopper with an inductive load. The simulations are performed according to the main parameters such as bus-voltage ($V_{\mathrm{DC}}$), commutated current ($I_{\mathrm{ds}}$), junction temperature ($T_j$), gate-voltage ($V_{gs}$), gate-resistances ($R_{\mathrm{gON}}$ and $R_{\mathrm{gOFF}}$), and the circuit elements (capacitors and loop-inductance). By adjusting the gate-resistance and the gate control voltage, the simulations give the same switching speeds as observed in practice. Also, the various parasitic capacitances which take into account the different oscillations observed, were also identified.

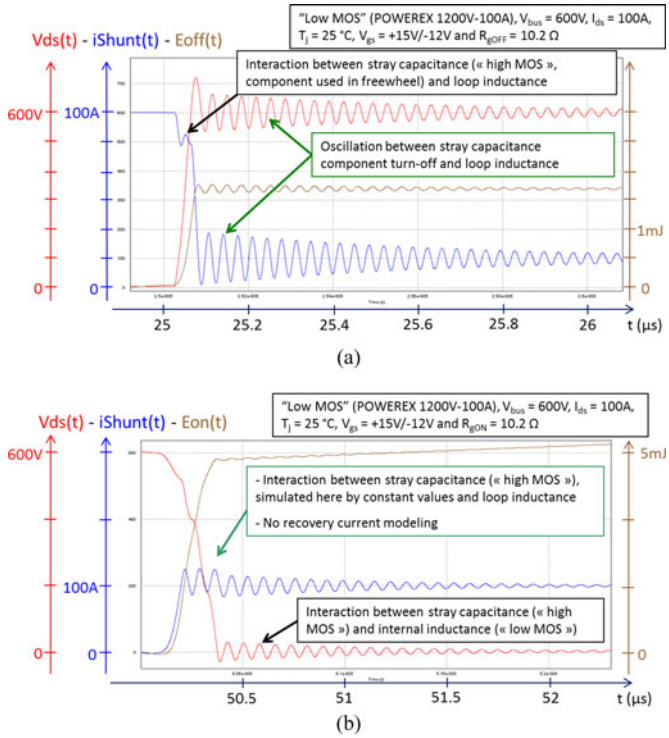


Fig. 3. Simulation results: dual-SiC MOSFET module (a) turn-off waveforms and (b) turn-on waveforms.

Fig. 3 shows an example of simulation results in which current, voltage, and energy waveforms are presented.

By comparing simulation results and measurements, the diode model was improved to include the small recovery current observed. In Fig. 4, this model is placed in a circuit to adjust the parameters of the recovery current.

Fig. 5 shows simulation results at diode turn-off: current, voltage, and energy waveforms are presented. These results are obtained with the circuit during a turn-on of the opposite MOSFET. The parameters for the recovery current are adjusted according to the experimentally obtained waveforms.

### B. Environmental Modeling of the Dual-SiC MOSFET Module to Design the Test-Bench

The main advantage of the new SiC-MOSFET modules comes from their high switching speed. Special care should be taken in circuit layout to minimize the loop-inductance (capacitors, bus-bar, and SiC-MOSFET module) [37–40]. Module construction and the connection to the dc-link capacitors have to be considered with regards to high-speed switching and high-current capability to minimize voltage transients due to the high turn-off *di/dt*, which could destroy the SiC device. Furthermore, oscillations that could cause EMC problems [41–44] have to be minimized. The challenge is therefore to achieve a bus-bar including a shunt current measurement with a loop-inductance as low as possible.

To assist in the design of various test benches, an innovative procedure, based on 3-D electromagnetic modeling, allows complete simulation of the electrical behavior of the

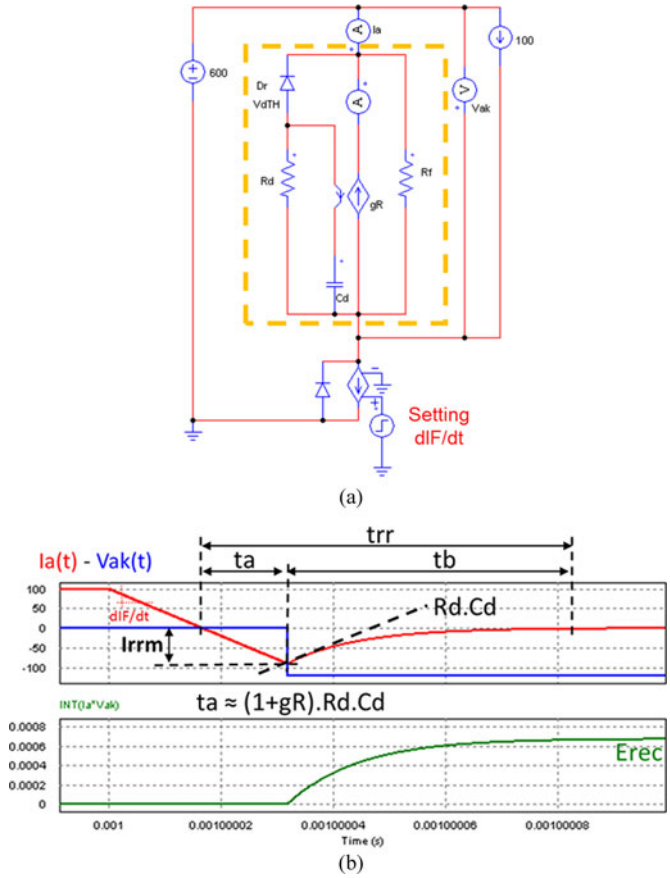


Fig. 4. (a) Test circuit for the 1200-V SiC Diode model. (b) Diode turn-off waveforms with recovery current.

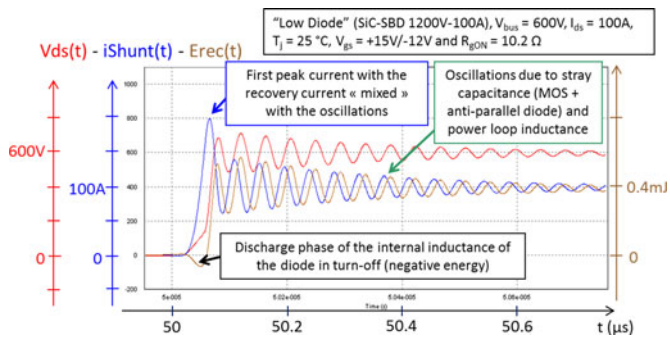


Fig. 5. Simulation results at diode turn-off: Current, voltage, and energy waveforms.

dc-capacitor/bus-bar connection/module-packaging circuit. Thus, it is even possible to optimize the position of the half-bridge power module. For that, a mechanical design of the entire test-bench was performed with SolidEdge (see Fig. 6). Then, a cosimulation with Q3D and Simplorer allowed taking into account all the assembly elements [45], [46] (see Fig. 7). In the simulations, internal stray inductances of the power modules were taken into account as well as the stray inductance of the driver circuit.

Using the flowchart of Fig. 8 to optimize the design of the power circuit, the iterations on different bus-bar designs led to a minimum stray inductance of less than 37 nH (internal inductance corresponding to the assembly of capacitors, connectors, and bus-bar). Table I and Fig. 9 show examples with three different designs and their impact on the SiC-MOSFET switching waveforms.

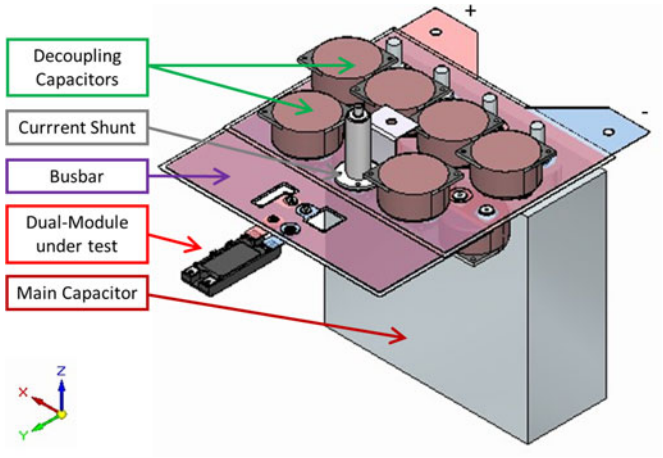


Fig. 6. Geometry design of the test-bench (SolidEdge Software).

## III. Switching Characterization of 1200 V-100 A Dual-SiC MOSFET Modules

### A. Test-Bench Principle and Implementation of SiC-MOSFET in Switching Cell

The circuit diagrams corresponding to the two possible configurations of the chopper with inductive load, are shown in Fig. 10. Unlike a conventional circuit used to characterize a silicon IGBT, special care was taken in the design of the circuit to minimize the loop-inductance between the bus capacitor and the SiC-MOSFET module (see Fig. 8). Each test-point allows the measurements of $V_{\rm ds}(t)$ and $I_{\rm ds}(t)$ on the controlled component. Gate-voltage $V_{\rm gs}(t)$ and gate-current $I_g(t)$ can also be measured to verify the correct operation of the driver. From $V_{\rm ds}(t)$ and $I_{\rm ds}(t)$ plots, switching energies, $E_{\rm off}(t)$, $E_{\rm on}(t)$, and $E_{\rm rec}(t)$, are obtained by integration of the product. Thus, the curves of switching energy versus switched current can be plotted for a fixed junction temperature and dc voltage, $V_{\rm DC}$.

As shown in Fig. 11, the switching characteristics were measured with a "classical" single or double-pulse pattern.

For SiC devices, the measurements require sensors with large bandwidths since switching energies are calculated from the product of current and voltage waveforms. The voltage $V_{\rm ds}(t)$ is measured with a passive probe (bandwidth ≤250 MHz), and the current $I_{\rm ds}(t)$ is measured with shunt (bandwidth ≤200 MHz). Fig. 12 shows a picture of the test-bench equipped with a SiC-MOSFET module and measurements devices.

### B. Switching Waveforms Analysis

A characterization procedure was carried out on several 1200 V-100 A dual-SiC MOSFET modules. For each module, the measurements were performed for a switched current ranging from 0 A to twice the nominal current ($2 \times I_{\rm n} = 200$ A).

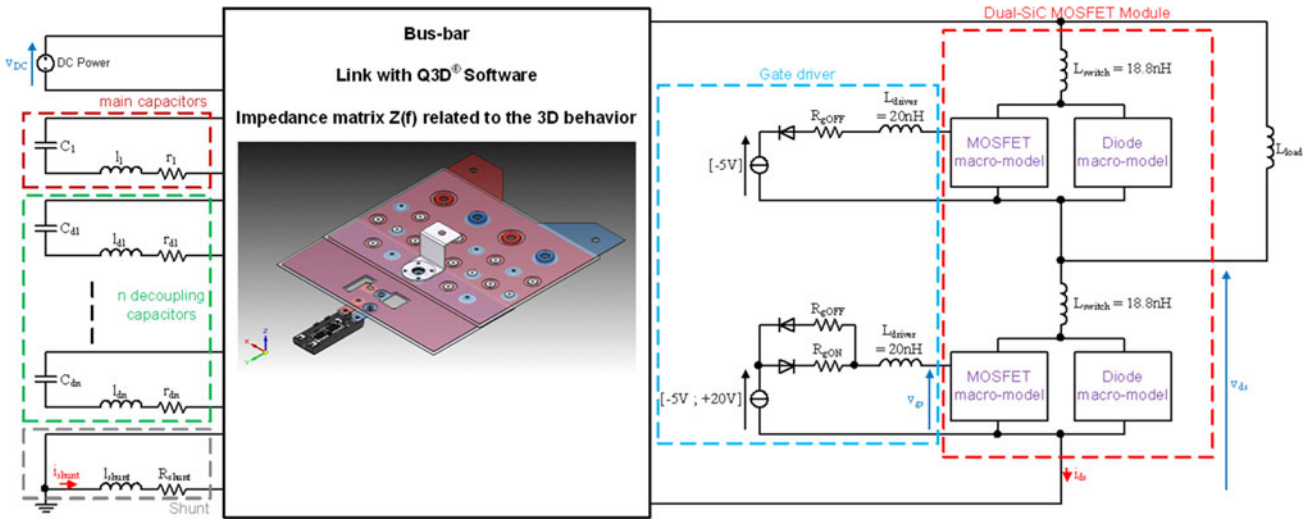


Fig. 7. Modeling of components in their environment (3-D electromagnetic and electric cosimulation using Q3D and Simplorer).

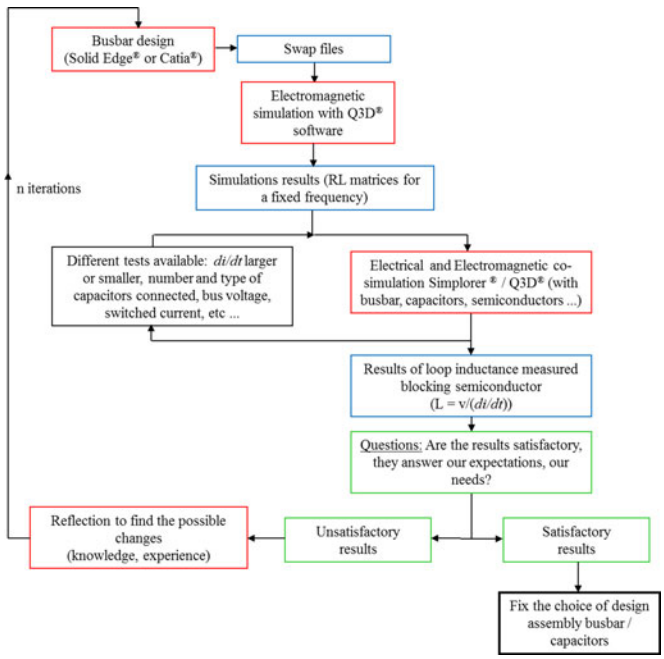


Fig. 8. Flowchart used to minimize the loop-inductance (3-D electromagnetic and electric cosimulation using Q3D and Simplorer).

DC bus voltages of 600, 750, and 900 V as well as junction temperatures of 25 °C, 125 °C, and 150 °C were considered. In this paper, the results are presented only for one dual-SiC MOSFET module, but it is important to note that the dynamic behaviors of the other tested modules are similar. To achieve an objective comparison, a 1200 V-100 A dual-Si Trench/Field-Stop IGBT module was also characterized in the same conditions. All the SiC-MOSFET and Si-IGBT curves presented in the following are synchronized with the gate voltage signal.

*1) Turn-Off Waveforms Analysis:* Fig. 13 shows an example of turn-off waveforms for $V_{\rm DC} = 600$ V, $I_{\rm load} = 200$ A, $T_j = 150$ °C, $V_{\rm gs} = +20{\rm V}/-5$ V, and $R_{\rm gOFF} = 3.5\ \Omega$ performed with the test circuit of Fig. 10(a).

TABLE I
RESULTS OF STUDY BY COSIMULATION: IMPACT OF BUS-BAR DESIGN ON THE SIC-MOSFET TURN-OFF

| Iterations designs | $V_{\rm ds\_max}$ (V) | $dI_{\rm ds\_off}/dt$ [10–90%] (kA/$\mu$s) | $L_{\rm power}$ (nH) (capacitors, connectors, and bus-bar) |
|---|---|---|---|
| Bus-bar n°1 (with bus-capacitor 1500 $\mu$F) | 933.7 | 3.17 | 86.5 |
| Bus-bar n°2 (with bus-capacitor 1500 $\mu$F and decoupling capacitors 4×47 $\mu$F) | 802.7 | 3.40 | 40.7 |
| Bus-bar n°3 (with bus-capacitor 1500 $\mu$F and decoupling capacitors 10 × 47 $\mu$F) | 792.4 | 3.47 | 36.7 |

For $V_{\rm DC} = 600$ V, $I_{\rm LOAD} = 200$ A, $T_J = 25$ °C, $V_{\rm GS} = +20{\rm V}/-5$ V, $R_{\rm GOFF} = 3.5\ \Omega$, and $R_{\rm GON} = 2.5\ \Omega$.

These waveforms show that the turn-off energy of the SiC MOSFET is lower than that of the Si-IGBT with the same rating. Furthermore, it was found that under similar electrical operating conditions, *dv/dt*, *di/dt*, and switching losses are almost independent of junction temperature for SiC MOSFETs which is not the case for Si-IGBTs whose switching losses increase with temperature. On the other hand, the high turn-off *di/dt* of the SiC devices leads to a higher overvoltage than for the IGBT which shows a tail current at turn-off. Current and voltage oscillations are due to the resonant circuit formed by the loop-inductance and stray capacitances of the semiconductors. The overvoltage at turn-off is a combination of these oscillations and the effect of *di/dt*.

*2) Turn-On Waveforms Analysis:* Fig. 14 shows an example of turn-on waveforms for $V_{\rm DC} = 600$ V, $I_{\rm load} = 200$ A, $T_j = 150$ °C, $V_{gs} = +20$ V$/-5$ V, and $R_{\rm gON} = 2.5\ \Omega$ and performed with the test circuit of Fig. 10(a).

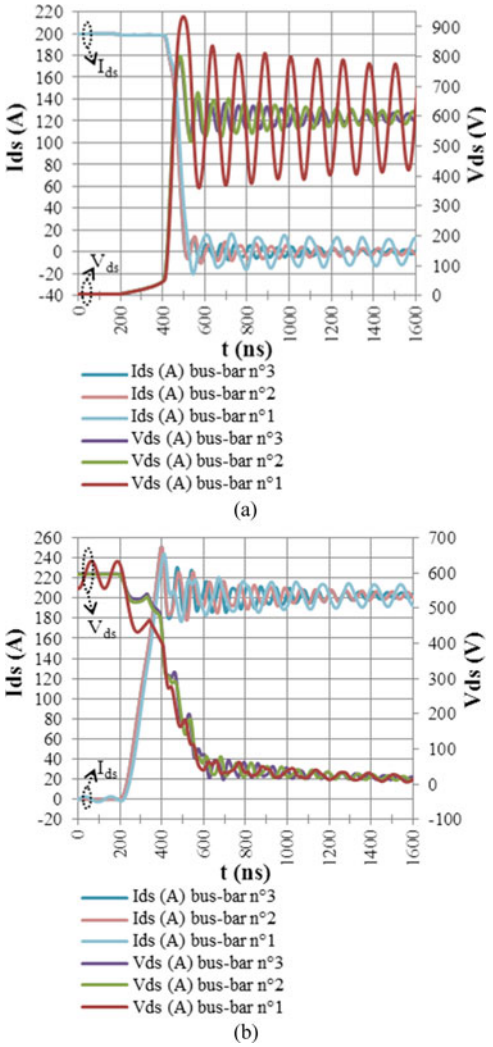


Fig. 9. Results of cosimulations—impact of bus-bar design on the switching waveforms (for $V_{\mathrm{DC}} = 600$ V, $I_{\mathrm{load}} = 200$ A, $T_j = 25\ ^{\circ}\mathrm{C}$, $V_{\mathrm{gs}} = +20$ V/$-5$ V, $R_{\mathrm{gOFF}} = 3.5\ \Omega$ and $R_{\mathrm{gON}} = 2.5\ \Omega$). (a) SiC-MOSFET turn-off. (b) SiC-MOSFET turn-on.

These waveforms show that the turn-on energy of the SiC-MOSFET is lower than that of the Si-IGBT with the same rating. As for the turn-off *dv/dt* and *di/dt,* these, again, are almost independent of the junction temperature, likewise, the switching losses. Unlike a conventional silicon module that contains p-i-n diodes, the SiC dual-pack contains Schottky barrier diodes (SBD) which theoretically have no recovery current. Nevertheless, it should be noted that the SBD shows a small reverse current peak for high *di/dt* values. As for turn-off, the current and voltage oscillations are due to the resonant circuit formed by the loop-inductance and stray capacitances of the semiconductor (capacitances of the MOSFET and antiparallel SBD).

*3) Comparison Between SiC-MOSFET Module and Si-IGBT Module:* Table II shows a comparison of switching performances for a given operating point: $V_{\mathrm{DC}} = 600$ V, $I_{\mathrm{load}} = 200$ A, $T_j = 150\ ^{\circ}\mathrm{C}$, $V_{\mathrm{gs}} = +20\ V/-5\ V$, $R_{\mathrm{gOFF}} = 3.5\ \Omega$, and $R_{\mathrm{gON}} = 2.5\ \Omega$.

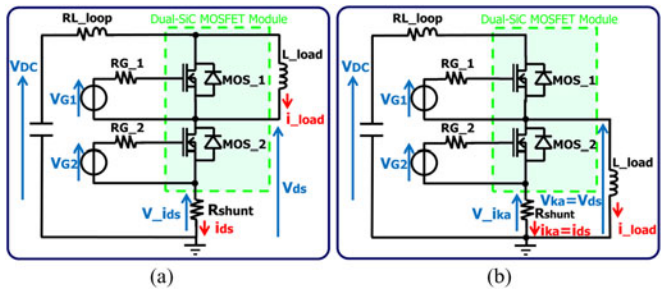


Fig. 10. Circuit for the switching characterization of dual-SiC MOSFET modules, (a) SiC MOSFET turn-off and turn-on, (b) SiC diode turn-off.

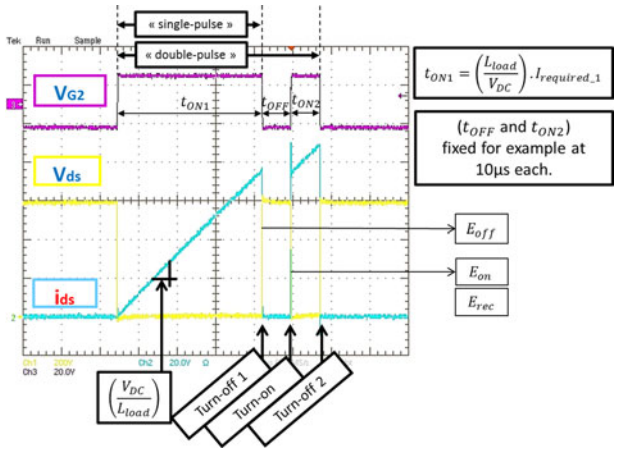


Fig. 11. Single- or double-pulse control for switching characterization.

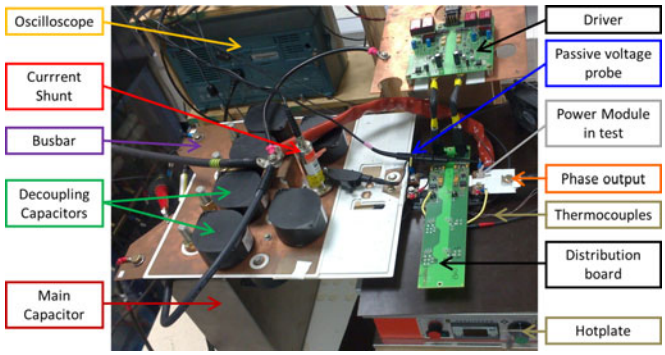


Fig. 12. Test-bench equipped with SiC MOSFET module.

As shown in Fig. 15, the switching energies of the SiC module are dramatically lower than those of the equivalent Si-IGBT module. At nominal current and $T_j = 150\ ^{\circ}\mathrm{C}$, the reduction is a factor of about 11 at turn-off and about 4 at turn-on; the recovery energy of the Schottky diode is about 36 times lower than that of the p-i-n diode.

## IV. Dual-SiC MOSFET Modules Characterization by Using the Opposition Method

Once the characterization was completed, it was interesting to compare semiconductor losses in the VSI operation.

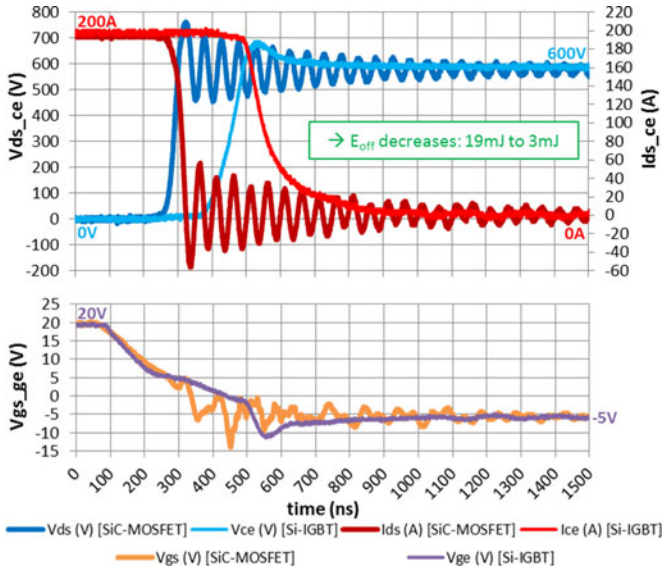


Fig. 13. Experimental turn-off waveforms (current and voltage).

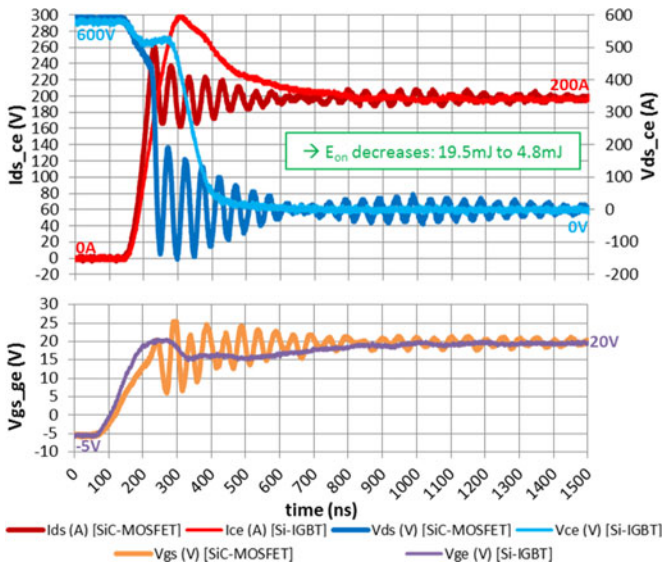


Fig. 14. Experimental turn-on waveforms (current and voltage).

TABLE II
COMPARISON OF DIFFERENT TIMES AND SWITCHING SPEEDS BETWEEN SIC-MOSFET MODULE AND SI-IGBT MODULE

| $V_{\rm DC}$ = 600 V, $I_{\rm load}$ = 200 A, $T_j$ = 150 °C, $V_{\rm gs}$ = +20 V/−5 V, $R_{\rm gOFF}$ = 3.5 Ω and $R_{\rm gON}$ = 2.5 Ω | | Si-IGBT | SiC-MOSFET |
|---|---|---|---|
| **Turn-off** | $t_{\rm doff}$ (ns) | 294 | 169.4 |
| | $t_f$ (ns) | 92.6 | 30.8 |
| | $t_{\rm off}$ (ns) | 386.6 | 200.2 |
| | $dV_{\rm ds\_ce\_off}/dt$ [10–90%] (kV/μs) | 5.2 | 15.6 |
| | $dV_{\rm ds\_ce\_off}/dt$ max (kV/μs) | 6.0 | 20.0 |
| | $V_{\rm ds\_ce}$ max (V) | 686.3 | 762.1 |
| | $dI_{\rm ds\_ce\_off}/dt$ [10–90%] (kA/μs) | −0.8 | −3.9 |
| | $dI_{\rm ds\_ce\_off}/dt$ max (kA/μs) | −2.9 | −6.0 |
| **Turn-on** | $t_{\rm don}$ (ns) | 86 | 66 |
| | $t_r$ (ns) | 224 | 71.5 |
| | $t_{\rm on}$ (ns) | 310 | 137.5 |
| | $dV_{\rm ds\_ce\_on}/dt$ [10–90%] (kV/μs) | –2.1 | –6.7 |
| | $dV_{\rm ds\_ce\_on}/dt$ max (kV/μs) | −5 | −20.0 |
| | $I_{\rm ds\_ce}$ max (A) | 299.7 | 263.3 |
| | $dI_{\rm ds\_ce\_on}/dt$ [10–90%] (kA/μs) | 2.5 | 3.5 |
| | $dI_{\rm ds\_ce\_on}/dt$ max (kA/μs) | 2.6 | 5.0 |

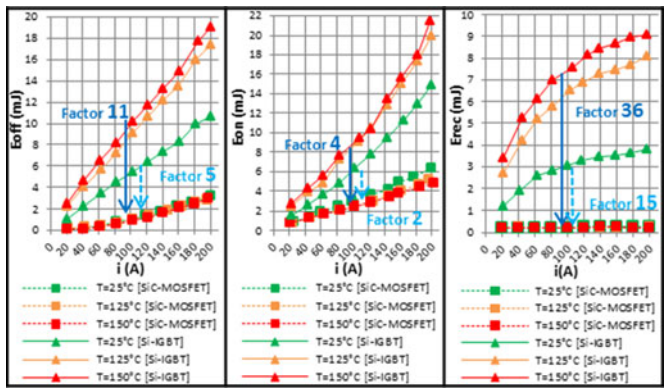


Fig. 15. Energy versus commutated current, (a) turn-off, (b) turn-on, (c) antiparallel diode turn-off—Comparison between SiC-MOSFET and Si-IGBT.

### A. Principle

As shown in Fig. 16, an opposition method test-bench, based on an H-bridge supplying an inductor, was built. In this circuit, one leg imposes the voltage while the other one assures current flow [34–36]. This test-bench allows the investigation of all operating points, in inverter or chopper mode, according to several parameters such as bus voltage ($V_{\rm DC}$), load current ($I_{\rm opp}$), modulation frequency ($f_{\rm mod}$), switching frequency ($f_{\rm sw}$), dead time ($t_{\rm m}$), phase-shift between current and voltage ($\varphi$), gate-voltage ($V_{\rm gs}$), and gate resistors ($R_{\rm gON}$ and $R_{\rm gOFF}$). Beyond that, the opposition method allows the characterization of power semiconductors in real working conditions since the mechanical design of bus bars and the thermal environment (cooling system) are also taken into account.

In addition, this test-bench was used to study the direct parallel connection of power modules to reach the high current capability required by traction applications. In the test procedure, the total losses in the modules are evaluated in PWM-VSI mode by using two methods: measuring the electrical input power *and* calorimetry of the cooling water.

### B. Measurement of Losses by the Electrical Method

The power measurement at the dc link gives the total losses of the system (see Fig. 16). The losses in the input filter ($L_{\rm filter}$ and $C_{\rm bus}$) were considered negligible whereas those of the air-cored inductor, $L_{\rm opp}$ and its connecting cables were calculated after characterization with an impedance bridge. The losses in the inverter legs are then determined by subtracting the load inductor losses from the input power. The losses in one leg can be derived if an operating point with symmetrical conditions is respected ($\varphi = \pi/2$) [34]. For unsymmetrical operating conditions, it is necessary to know the losses of one leg before determining the losses on the second leg. Finally, tests were carried out

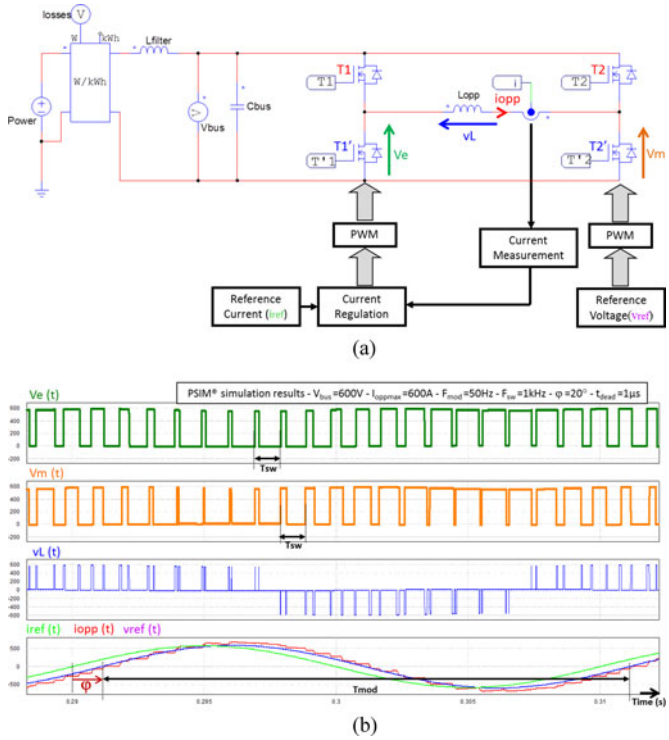


Fig. 16. Opposition method principle with an H-Bridge (PWM-VSI mode), (a) Schematic diagram, (b) Simulation results for one period.

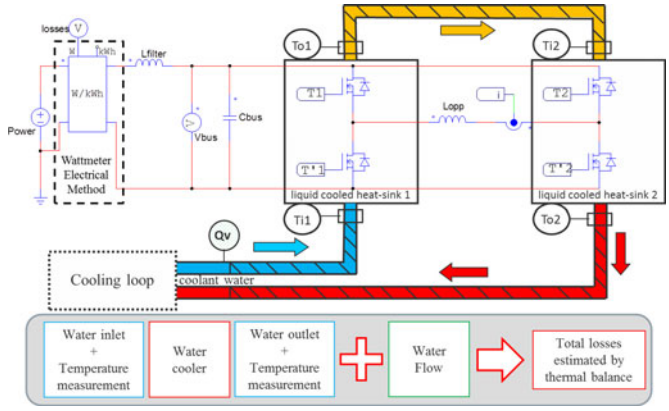


Fig. 17. Calorimetric method applied on the opposition test-bench.

at different switching frequencies to separate conduction and switching losses.

### C. Measurement of Losses by the Calorimetric Method

As shown in Fig. 17, the thermal method consists of measuring the coolant flow rate and the input and output temperatures [47], [48]. To ensure adiabatic conditions, the coolers are insulated with foam. To obtain accurate temperatures, measurements are performed by probes PT100 Class B/10 (Ti1, To1, Ti2, and To2), and the flow is measured by a flow-meter with a vortex system (Qv). Nevertheless, the accuracy of the power-losses measurement depends on the differential temperature, and a reduction of the flow rate is required to obtain an accurate

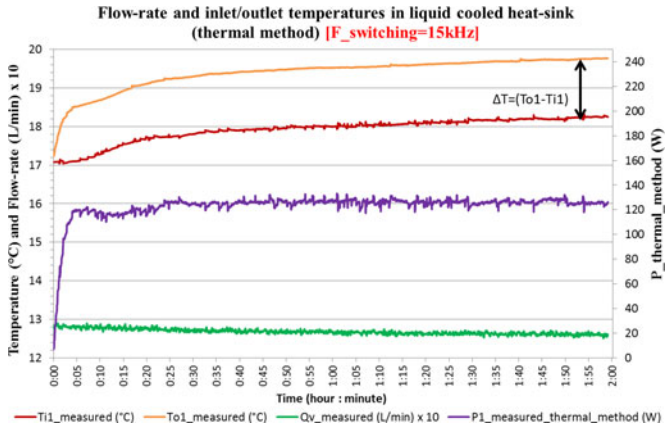


Fig. 18. Heat-sink 1; flow-rate and inlet/outlet temperatures recording for a SiC-MOSFET module.

measurement for operating points with low losses (in our case, the minimum flow was 0.5 L/min).

Equation (1) gives the expression of switching losses in a leg as a function of thermodynamic parameters

$$P_{\text{leg}} = \rho \times Q_v \times C_p \times (\Delta T_o - \Delta T_i) \tag{1}$$

where:

$P_{\text{leg}}$ total losses per leg [W];
$(\Delta T_o - \Delta T_i)$ differential temperature of cooling water between the output and the input of the heat-sink [°K];
$\rho$ density of the coolant [kg/m$^3$];
$C_p$ specific heat capacity of cooling water [J/(kg.K)];
$Q_v$ flow rate of cooling water [m$^3$/s].

Thermocouple sensors were placed under the base-plate of the power modules in order to estimate the junction temperature of the chips. Temperatures and flow rates were recorded on a data logger. Before using SiC-MOSFET devices, a first stage of validation and calibration of the two methods was performed with Si-IGBT 1200 V-100 A modules.

As an example, the measurements presented in Fig. 18 for Heat-sink 1 equipped with a SiC-MOSFET module, were recorded over 2 h with a sampling rate of one per second. In this example, the cooling loop tries to maintain a constant flow of about 1.25 L/min, while the heat-sink temperatures (inlet/outlet) evolve, resulting in a loss estimation that is stabilized after 30 min of operation.

### D. Details of the Implemented Test-Bench

The key parameters which fix the operating range of the test-bench are listed as follows:

1) DC Bus Voltage : 0 to 1100 V;
2) number of modules in parallel: 1 to 3 (here with 1200 V-100 A dual-SiC MOSFET modules or 1200 V-100 A dual-Si IGBT modules);
3) output sine-wave current : 0 to 600 A peak;
4) fundamental frequency : 0 to 500 Hz;
5) current phase-shift $\varphi$ : 0 to $\pi$;
6) switching frequency : 1 to 20 kHz, by step of 1 kHz;

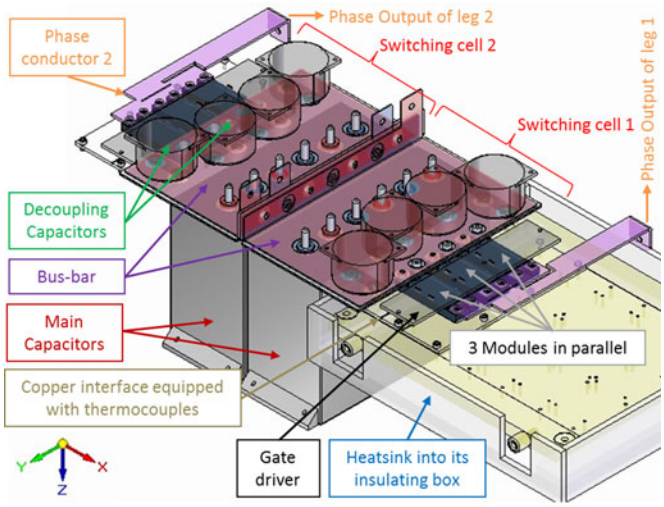


(a)

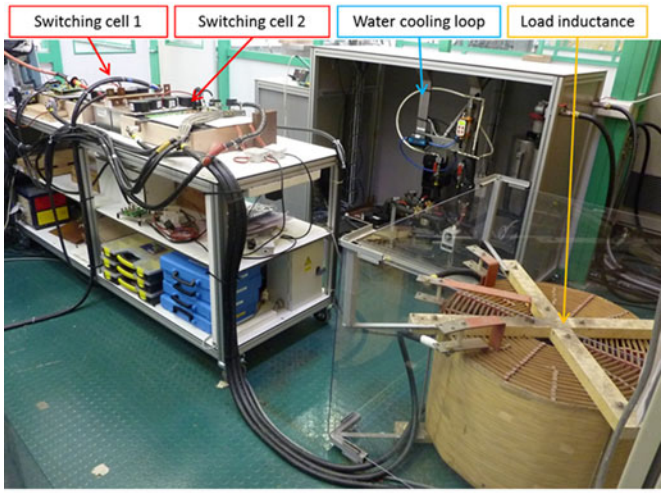


(b)

Fig. 19. Opposition test-bench, (a) mechanical design (SolidEdge), (b) picture of the test-bench.

7) modulation ratio adjustable independently of each leg: 0.1 to 0.9;
8) minimum dead time: 2 $\mu$s, here dead time: 3 $\mu$s;
9) water-flow cooling system : 0.5 to 5 L/min;
10) maximum power dissipation: 5 kW.

Fig. 19 shows the mechanical design and a picture of the opposition test-bench.

## V. Estimation of Losses—Comparison of Different Methods and Comparison of SiC-MOSFET Versus Si-IGBT Modules

In this section, the semiconductor losses are determined by using the two methods mentioned previously. Furthermore, these results were compared with calculations based on the on-state characteristics and switching energies previously determined with a pulse test-bench.

Fig. 20 recalls the first approach used to estimate semiconductor losses in inverter operation. First, the SiC-MOSFET on-state

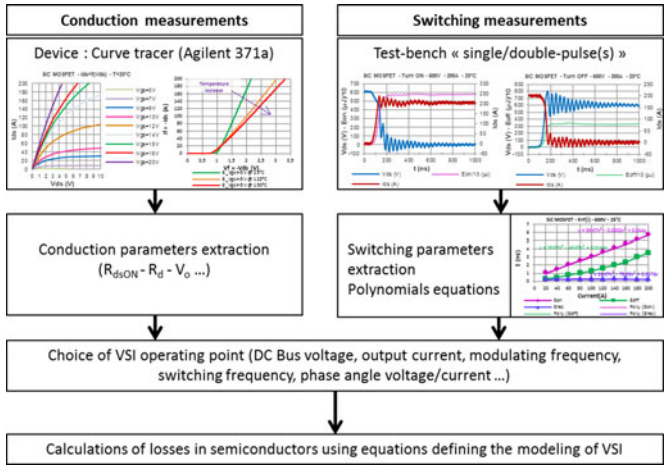


Fig. 20. Calculation of losses based on conduction and switching characteristics (analytical method).

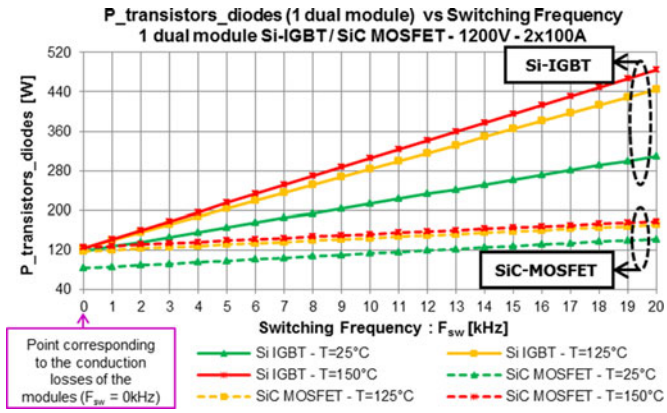


Fig. 21. Losses comparison between 1200 V-100 A Si-IGBT and SiC-MOSFET modules versus switching frequency for three junction temperatures.

TABLE III
VSI Parameters

| | |
|---|---|
| VSI control | PWM |
| Modulation ratio | 0.5 |
| Junction Temperature | [25/125/150] °C |
| DC Bus Voltage | 600 V |
| Output Current | Sinusoidal waveform<br>100 A peak /50 Hz<br>Phase angle $\varphi = \pi/2$ |
| Switching frequency | [0–20] kHz by step 1 kHz |

resistance (in forward and reverse directions) and the antiparallel SiC-Diode slope-resistance and threshold-voltage were extracted from conduction tests. Switching energies from single and double-pulse tests (see Fig. 11) were represented by polynomial equations. Using these parameters, the calculation of semiconductor losses was performed. In this calculation, contrary to the Si-IGBT which is unidirectional, the reverse conduction of the SiC-MOSFET was considered. All equations were implemented in a specific calculation routine. It should

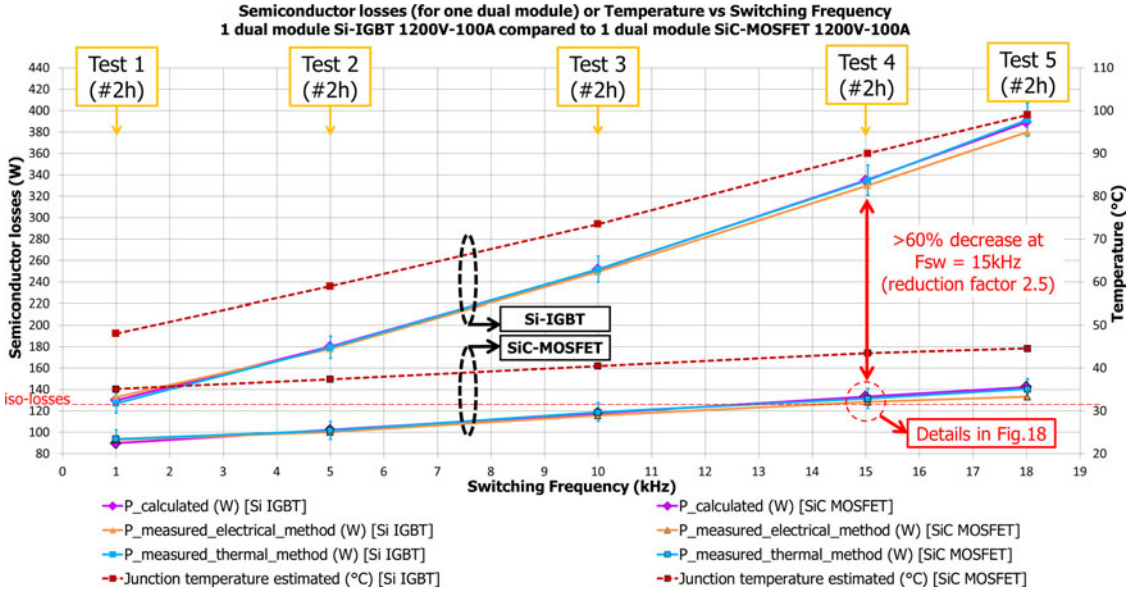


Fig. 22. VSI operation. Total dissipated Power (transistor + diode) versus switching frequency. Comparison between SiC-MOSFET and Si-IGBT modules.

TABLE IV
VSI PARAMETERS

| | |
|---|---|
| VSI control | PWM |
| Modulation ratio | 0.5 |
| Junction Temperature | [25/125/150] °C |
| DC Bus Voltage | 600 V |
| Output Current | Sinusoidal waveform<br>100 A peak/20 Hz<br>Phase angle $\varphi = \pi/2$ |
| Switching frequency | [1–18] kHz |
| Dead time | 3 $\mu$s |

be noted that the gate drivers used in the two test benches are the same.

Fig. 21 shows an example obtained with this calculation routine. It allows a comparison between the 1200 V-100 A Si-IGBT and SiC-MOSFET modules, the total losses (transistor and diode) versus switching frequency are given for three junction temperatures under the conditions of Table III.

For this calculation approach, the estimation of junction temperature and the resulting losses are performed by successive iterations which take into consideration the temperature measurement at the base of the power module (considered as "Case Temperature").

Fig. 22 shows the results obtained on Heat-sink 1 (see Fig. 17), this is a comparison between a Si-IGBT module and a SiC-MOSFET module under the conditions of Table IV.

In Fig. 22, the points corresponding to the thermal method are shown by bars for each switching frequency point. These bars represent measurement uncertainties. Accuracy increases with the number of modules in parallel (i.e., at higher powers) as the water temperature differential increases.

The measurement results show that the calculated losses are correct since calorimetry is subject only to well-defined errors (mainly $\Delta T$). For the SiC-MOSFET, it confirms the accuracy of current and voltage measurements during switching tests and validates the on-state modeling of the SiC-MOSFET which takes into account the current bidirectionality. The calculation approach and the calorimetric method give almost the same result. This can be explained by the fact that the two test benches were designed with the same loop inductance values. On the other hand, the electrical method assumes the same losses in the modules but in our test bench, the precision is degraded by the series connection of the heat-sinks. Although the two modules operate at the same voltage and current level, the junction temperatures are not the same. As a consequence, the error in the loss estimation increases with the switching frequency. Nevertheless, it was observed that this error is always small (less than 4% at 15 kHz) even in the case of three modules in parallel on each leg and with 300 A of peak current (see Fig. 23).

Beyond the successful operation for the SiC-MOSFET modules, these results show a reduction in total losses (one dual module: transistors and diodes) of 60% for a switching frequency of 15 kHz. The Si-IGBT module at 1 kHz has the same losses as the SiC-MOSFET module at 15 kHz. Table V summarizes the results presented in Fig. 22.

Finally, a comparison based on the calculation method was performed in the case of a more conventional VSI operating point which is defined in Table VI. The results presented in Table VII show a reduction in total losses (one dual module: transistors and diodes) of 57% for a switching frequency of 20 kHz. It should be noticed that the losses at 1 kHz are lower in the Si-IGBT module than in the SiC-MOSFET module. In fact, for a current level greater than 50 A, the SiC-MOSFET shows a higher voltage drop than the Si-IGBT (at $T_j = 150\ ^\circ$C).

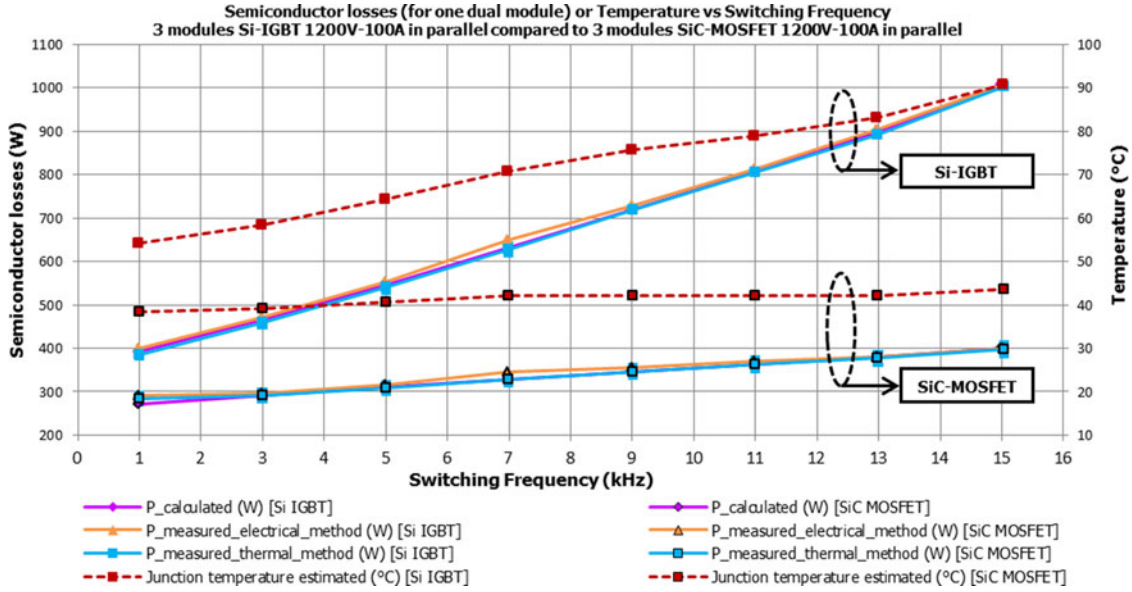


Fig. 23. VSI operation. Total dissipated power (for one dual module) versus switching frequency. Comparison between three SiC-MOSFET modules in parallel and three Si-IGBT modules in parallel.

TABLE V
POWER LOSS COMPARISON: SIC-MOSFET VERSUS SI-IGBT

| $F_{sw}$ (kHz) | Total Power Losses in a dual module 1200 V-100 A (W) | | Losses reduction (%) [equation: $(P_{SiC}/P_{Si}-1).100$] |
|---|---|---|---|
| | Si-IGBT | SiC-MOSFET | |
| 1 | 128 | 95 | –25.8 |
| 5 | 180 | 100 | –44.4 |
| 10 | 250 | 113 | –54.8 |
| 15 | 330 | 132 | –60.0 |

TABLE VI
VSI PARAMETERS

| | |
|---|---|
| VSI control | PWM |
| Modulation ratio | 0.9 |
| Junction Temperature | 150 °C |
| DC Bus Voltage | 600 V |
| Output Current | Sinusoidal waveform |
| | 100 A peak/20 Hz |
| | Phase angle $\varphi = 20\ °$ ($\cos(\varphi) \approx 0{,}94$) |
| Switching frequency | [1–5–10–15–20] kHz |

TABLE VII
POWER LOSS COMPARISON: SIC-MOSFET VERSUS SI-IGBT

| $F_{sw}$ (kHz) | Total Power Losses in a dual module 1200 V-100 A (W) | | Losses reduction (%) [equation : $(P_{SiC}/P_{Si}-1).100$] |
|---|---|---|---|
| | Si-IGBT | SiC-MOSFET | |
| 1 | 149 | 158 | +6.5 |
| 5 | 221 | 169 | −23.5 |
| 10 | 311 | 182 | −41.4 |
| 15 | 400 | 195 | −51.3 |
| 20 | 490 | 208 | −57.6 |

## VI. CONCLUSION

In railway traction, where low mass and volume is a necessity, the lower converter losses will minimize the size of the cooling system or even change its technology, especially since SiC components allow far greater junction temperature limits. It is also possible to increase switching frequency to reduce the size of the passive filtering components. However, many challenges remain in order to use these components, including understanding the effects on EMC of oscillations during switching, learning to drastically reduce inductance loops (power and control side) [37–40] and studying the effects of high *dv/dt* on the insulation of traction motor windings [41–44].

Another hurdle to overcome in the use of these components in railway traction is the availability of higher current-caliber modules making it necessary to develop new module technology that allows the parallel connection of a large number of chips [49]. The study of the gate-signal distribution from driver to the different gate chips is also important.

In this paper, we have seen the advantages of comprehensive modeling and optimization of the switching cell including capacitors, bus-bar, and power module as opposed to considering the different elements of the switching cell independently [50], [51]; only in this way will high switching speeds and high currents be achieved.

Two test-benches were used: The first one operating on the principle of single or double pulse was used to study the switching behavior of the devices and the second one, operating as a VSI, was based on an opposition method. It demonstrated the feasibility of an inverter leg operating at high current and high switching frequency. This test-bench was developed to evaluate the performances of SiC-MOSFET modules for future use in railway converters. Experimental results validated the electrical and thermal measurement methods. In addition, hundreds of hours in inverter mode with SiC-MOSFET devices

were cumulated. The experimental results show a significant reduction of semiconductor losses and confirm the possibility of increased switching frequency; the combination of these two advantages will have an impact at system level. Loss reduction in static converters will lead to reductions in the cooling system size or even change its technology altogether, especially since SiC components allow higher junction temperatures [16–18]. Moreover, higher frequency will reduce the size of passive filters or allow different motor-control strategies [52]. Generally speaking, the introduction of SiC components requires a review of the entire design of the traction chain to obtain significant reduction in mass and volume and to facilitate integration. For the moment, the target applications are auxiliary converters but the upcoming 1700-V SiC devices will allow the design of traction inverters for subways and streetcars.

## REFERENCES


[1] B. J. Baliga, M. S. Adler, P. V. Gray, R. P. Love, and N. Zommer, "The insulated gate rectifier (IGR): A new power switching device," *IEDM Tech. Dig.*, vol. 28, pp. 264–267, 1982.

[2] J. P. Russell, A. M. Goodman, L. A. Goodman, and J. M. Neilson, "The COMFET—A new high conductance MOS-gates device," *IEEE Electron Device Lett.*, vol. EDL-4, no. 3, pp. 63–65, Mar. 1983.

[3] M. Debruyne, "High power IGBT traction drives," presented at the World Conf. Railway Res., Cologne, Germany, Nov. 2001.

[4] R. Hermann, E. U. Krafft, and A. Marz, "Reverse-conducting-IGBTs - A new IGBT technology setting new benchmarks in traction converters," in *Proc. 15th Eur. Conf. Power Electron. Appl.*, Lille, France, Sep. 2013, pp. 1–8.

[5] T. Minato, S. Aono, K. Uryu, and T. Yamaguchi, "Making a bridge from SJ-MOSFET to IGBT via RC-IGBT structure concept for 600 V class SJ-RC-IGBT in a single chip solution," in *Proc. 24th Int. Symp. Power Semicond. Devices ICs*, Bruges, Belgium, Jun. 2012, pp. 137–140.

[6] L. Storasta, A. Kopta, and M. Rahimo, "A comparison of charge dynamics in the reverse-conducting RC IGBT and Bi-mode Insulated Gate Transistor BiGT," in *Proc. 22nd Int. Symp. Power Semicond. Devices ICs*, Hiroshima, Japan, Jun. 2010, pp. 391–394.

[7] G. Majumdar, "Advanced power semiconductor technologies for efficient energy conversion," in *Proc. 13th Int. Workshop IEEE Junction Technol.*, Kyoto, Japan, Jun. 2013.

[8] X. Zhuxian, L. Ming, W. Fei, and L. Zhenxian, "Investigation of Si IGBT Operation at 200 °C for traction applications," *IEEE Trans. Power Electron.*, vol. 28, no. 5, pp. 2604–2615, May 2013.

[9] P. Kleinichen, R. Alvarez, M. Buschendorf, and S. Bernet, "Turn-on loss reduction of 6.5 kV/500 A trench/field-stop IGBTs using a simple GDU," in *Proc. IEEE Energy Convers. Congr. Expo.*, Denver, CO, USA, Sep. 2013, pp. 3671–3678.

[10] J. G. Bauer, T. Duetemeyer, and L. Lorenz, "New IGBT development for traction drive and wind power," in *Proc. Int. IEEE Power Electron. Conf.*, Jun. 2010, pp. 768–772.

[11] J. Millan, "A review of WBG power semiconductor devices," in *Proc. Int. Semicond. Conf.*, Oct. 2012, vol. 1, pp. 57–66.

[12] L. D. Stevanovic, K. S. Matocha, P. A. Losee, J. S. Glaser, J. J. Nasadoski, and S. D. Arthur, "Recent advances in silicon carbide MOSFET power devices," in *Proc. 25th Annu. IEEE Appl. Power Electron. Conf. Expo.*, Feb. 2010, pp. 401–407.

[13] D. C. Patel, A. Kadavelugu, S. Madhusoodhanan, S. Bhattacharya, K. Hatua, S. Leslie, S.-H. Ryu, D. Grider, A. Agarwal, "15 kV SiC IGBT based three-phase three-level modular-leg power converter," in *Proc. IEEE Energy Convers. Congr. Expo.*, Sep. 2013, pp. 3291–3298.

[14] S. Madhusoodhanan, K. Hatua, S. Bhattacharya, S. Leslie, R. Sei-Hyung, M. Das, A. Agarwal, D. Grider, "Comparison study of 12 kV n-type SiC IGBT with 10 kV SiC MOSFET and 6.5 kV Si IGBT based on 3L-NPC VSC applications," in *Proc. IEEE Energy Convers. Congr. Expo.*, Raleigh, NC, USA, Sep. 2012, pp. 310–317.

[15] Y. Du, J. Wang, G. Wang, and A. Q. Huang, "Modeling of the high-frequency rectifier with 10-kV SiC JBS diodes in high-voltage series resonant type DC-DC converters," *IEEE Trans. Power Electron.*, vol. 29, no. 8, pp. 4288–4300, Aug. 2014.

[16] R. Wang, D. Boroyevich, P. Ning, Z. Wang, F. Wang, P. Mattavelli, K. Ngo, and K. Rajashekara, "A high-temperature SiC three-phase ac-dc converter design for >100 °C ambient temperature," *IEEE Trans. Power Electron.*, vol. 28, no. 1, pp. 555–572, Jan. 2013.

[17] C. Raynaud, D. Tournier, H. Morel, and D. Planson, "Comparison of high voltage and high temperature performances of wide bandgap semiconductors for vertical power devices," *Diamond Related Mater*, vol. 19, no. 1, pp. 1–6, 2010.

[18] A. Lostetter, J. Hornberger, B. McPherson, B. Reese, R. Shaw, M. Schupbach, B. Rowden, A. Mantooth, J. Balda, T. Otsuka, K. Okumura, and M. Miura, "High-temperature silicon carbide and silicon on insulator based integrated power modules," in *Proc. IEEE Veh. Power Propul. Conf.*, 2009, pp. 1032–1035.

[19] C. DiMarino, Z. Chen, D. Boroyevich, R. Burgos, and P. Mattavelli, "Characterization and comparison of 1.2 kV SiC power semiconductor devices," in *Proc. Eur. Conf. Power Electron. Appl.*, Sep. 2013, pp. 1–10.

[20] M. Mermet-Guyennet, A. Castellazzi, J. Fabre, P. Ladoux, "Electrical analysis and packaging solutions for high-current fast-switching sic components," in *Proc. Int. Conf. Integr. Power Electron. Syst.*, Nuremberg, Germany, Mar. 6–8, 2012.

[21] A. Rodriguez Alonso, M. Fernandez Diaz, D. G. Lamar, M. Arias Perez de Aspeitia, M. M. Hernando, and J. Sebastian, "Switching performance comparison of the SiC JFET and SiC JFET/Si MOSFET cascode configuration," *IEEE Trans. Power Electron.*, vol. 29, no. 5, pp. 2428–2440, May 2014.

[22] P. Ladoux, M. Mermet-Guyennet, J. Casarin, and J. Fabre, "Outlook for SiC devices in traction converters," presented at the IEEE Int. Conf. Electr. Syst. Aircraft, Railway Ship Propul., Bologna, Italy, Oct. 16–18 2012.

[23] J. Casarin, P. Ladoux, B. Chauchat, D. Dedecius, and E. Laught, "Evaluation of high voltage SiC diodes in a medium frequency AC/DC converter for railway traction," in *Proc. Int. Symp. Power Electron. Electr. Drives Autom. Motion*, Sorrento, Italy, Jun. 2012, pp. 1182–1186.

[24] J. Biela, M. Schweizer, S. Waffler, and J. W. Kolar, "SiC versus Si—Evaluation of potentials for performance improvement of inverter and DC-DC converter systems by SiC power semiconductors," *IEEE Trans. Ind. Electron.*, vol. 58, no. 7, pp. 2872–2882, Jul. 2011.

[25] M. Mermet-Guyennet, "New power technologies for traction drives," in *Proc. IEEE Int. Symp. Power Electron. Electr. Drives Autom. Motion*, Pisa, Italy, Jun. 2010, pp. 719–723.

[26] S. Bernet, "Recent developments of high power converters for industry and traction applications," *IEEE Trans. Power Electron.*, vol. 15, no. 6, pp. 1102–1117, Nov. 2000.

[27] A. Merkert, T. Krone, and A. Mertens, "Characterization and scalable modeling of power semiconductors for optimized design of traction inverters with Si- and SiC-devices," *IEEE Trans. Power Electron.*, vol. 29, no. 5, pp. 2238–2245, May 2014.

[28] [Online]. Available: http://www.cree.com/

[29] [Online]. Available: http://www.rohm.com/

[30] Z. Liang, P. Ning, and F. Wang, "Development of advanced all-SiC power modules," *IEEE Trans. Power Electron.*, vol. 29, no. 5, pp. 2289–2295, May 2014.

[31] M. Horio, Y. Iizuka, and Y. Ikeda, "Packaging technologies for SiC power modules," *Fuji Electr. Rev.*, vol. 58, no. 2, pp. 75–80, Nov. 2011.

[32] T. Nakamura, M. Aketa, Y. Nakano, M. Sasagawa, and T. Otsuka, "Novel developments towards increased SiC power device and module efficiency," in *Proc. IEEE Energytech*, Cleveland, OH, USA,, May 29–31, 2012, pp. 1–6.

[33] J. Fabre, P. Ladoux, and M. Piton, "Characterization of SiC MOSFET dual modules for future use in railway traction chains," presented at the PCIM, Nuremberg, Germany, May 7–9, 2012.

[34] F. Forest, J.-J. Huselstein, S. Faucher, M. Elghazouani, P. Ladoux, T. A. Meynard, F. Richardeau, and C. Turpin, "Use of opposition method in the test of high-power electronic converters," *IEEE Trans. Ind. Electron.*, vol. 52, no. 2, pp. 530–541, Apr. 2006.

[35] B. Cougo, H. Schneider, and T. Meynard, "Accurate switching energy estimation of wide bandgap devices used in converters for aircraft applications," in *Proc. Eur. Conf. Power Electron. Appl.*, Sep. 2013, pp. 1–10.

[36] J. Fabre, P. Ladoux, and M. Piton, "Opposition method based test bench for characterization of SiC Dual MOSFET Modules," presented at the PCIM'13, Nuremberg, Germany, May 14–16, 2013.

[37] R. Bayerer and D. Domes, "Power circuit design for clean switching," in *Proc. 6th Int. Conf. Integr. Power Electron. Syst.*, Nuremberg, Germany, Mar. 2010, pp. 1–6.

[38] E. Batista and J. M. Dienot, "EMC characterization for switching noise investigation on power transistors," in *Proc. IEEE EMC Detroit Symp.*, Detroit, MI, USA, Aug. 2008, pp. 1–7.
[39] J. M. Dienot and E. Batista, "EM-Matrix antenna for real-time measurements of electromagnetic noise in power electronic modules," in *Proc. Antennas Propag. Conf.*, 2009, pp. 753–756.
[40] C. Chen, X. Pei, Y. Chen, and Y. Kang, "Investigation, evaluation, and optimization of stray inductance in laminated busbar," *IEEE Trans. Power Electron.*, vol. 29, no. 7, pp. 3679–3693, Jul. 2014.
[41] N. Oswald, P. Anthony, N. McNeill, and B. H. Stark, "An experimental investigation of the tradeoff between switching losses and EMI generation with hard-switched All-Si, Si-SiC, and all-SiC device combinations," *IEEE Trans. Power Electron.*, vol. 29, no. 5, pp. 2393–2407, May 2014.
[42] T. R. Mukundan, "Calculation of voltage surges on motors fed from PWM drives—A simplified approach," *IEEE Trans. Energy Convers.*, vol. 19, no. 1, pp. 223–225, Mar. 2004.
[43] G. L. Skibinski, R. J. Kerkman, and D. Schlegel, "EMI emissions of modern PWM AC drives," *IEEE Ind. Appl. Mag.*, vol. 5, no. 6, pp. 47–81, Nov./Dec. 1999.
[44] R. Robutel, C. Martin, C. Buttay, H. Morel, P. Mattavelli, D. Boroyevich, and R. Meuret, "Design and implementation of integrated common mode capacitors for SiC-JFET inverters," *IEEE Trans. Power Electron.*, vol. 29, no. 7, pp. 3625–3636, Jul. 2014.
[45] E. Batista, J. M. Dienot, M. Mermet-Guyennet, A. Castellazzi, "Accurate mixed electrical and electromagnetic model of a 6, 5 kV IGBT module," in *Proc. 7th Int. Conf. IEEE Power Electron.*, 2007, pp. 1151–1155.
[46] J. M. Dienot, E. Batista, and L. Bouchelouk, "Investigations and simulation of electromagnetic behavior in 3D hybrid electronic devices for embedded applications," presented at the Eur. Electromagn. Conf., Lausanne, Switzerland, 2008.
[47] M. Sverko and S. Krishnamurthy, "Calorimetric loss measurement system for air and water cooled power converters," in *Proc. 15th Eur. Conf. IEEE Power Electron. Appl.*, 2013, pp. 1–10.
[48] D. Christen, U. Badstuebner, J. Biela, J. W. Kolar, "Calorimetric power loss measurement for highly efficient converters," in *Proc. Int. Power Electron. Conf.*, Jun. 2010, pp. 1438–1445.
[49] T. A. Salem and R. A. Wood, "1000-H evaluation of a 1200-V, 880-A all-SiC dual module," *IEEE Trans. Power Electron.*, vol. 29, no. 5, pp. 2192–2198, May 2014.
[50] M. A. Brubaker, H. C. Kirbie, and T. A. Hosking, "Integrated DC link capacitor/bus structures to minimize external ESL contribution to voltage overshoot," in *Proc. IEEE Transp. Electrification Conf.*, Dearborn, MI, USA, Jun. 2012, pp. 1–6.
[51] S. Edward, "Low inductance–low temp rise DC bus capacitor properties enabling the optimization of high power inverters," in *Proc. PCIM Europe*, Nuremberg, Germany, May 4–6, 2010, pp. 75–80.
[52] J. Lemmens, P. Vanassche, and J. Driesen, "Optimal control of traction motor drives under electrothermal constraints," *IEEE J. Emer. Sel. Topics Power Electron.*, vol. 2, no. 2, pp. 249–263, Jun. 2014.

**Joseph Fabre** was born in Carcassonne, France, in 1985. He received the Engineering Degree in electrical engineering from ENSEEIHT (Ecole Nationale Superieure d'Electronique, d'Electrotechnique, d'Informatique, d'Hydraulique et de Telecommunications), Toulouse, France, in 2009, and the Ph.D. degree from the Institut National Polytechnique de Toulouse, Toulouse, France, and also from ALSTOM Transport Company at Power Electronics Technology team within Traction system engineering department, Tarbes, France, in 2013.

He is currently working on his postdoctorate project at the Static Converter Research Group at the Laboratoire Plasma et Conversion d'Energie, Toulouse. He is now involved in research programs on power electronics.

**Philippe Ladoux** (M'13) was born in France, in 1963. He received the Engineering degree in electrical engineering from Ecole Nationale Superieure d'Electronique, d'Electrotechnique, d'Informatique, d'Hydraulique et de Telecommunications, Toulouse, France, in 1987, and the Ph.D. degree from the Institut National Polytechnique de Toulouse, in 1992.

He is currently a Professor at the Institut National Polytechnique, where he teaches power electronics. From 2001 to 2009, he was a Manager of the Static Converters Research Group at Plasma et Conversion d'Energie, Toulouse. His research interests include high-power converters. He is now involved in research programs on power electronics for railway traction.

**Michel Piton** was born in France, in 1965. He received the Engineering degree in electrical engineering from E.N.S.I.E.G., Grenoble, France, in 1989.

He joined ALSTOM Transport in 1990 and participated to design of IGBT-based traction drives ONIX.

He was a Manager of traction converter and switchgear validation group and is currently responsible for Power Electronics Technology team within Traction System Engineering Department. His field of expertize is high-power semiconductors for railway traction.